國立雲林科技大學
101 學年度博士班招生考試試題

所別：化學工程與材料工程系
科目：科技文獻

一. 根據附件一，回答下列問題：

1. 請分別說明下列參數，影響超音波降解廢水中二硝基甲苯之趨勢及原因：

   (1) 超音波聲強度。(10%)

   (2) 廢水之酸度。(10%)

   (3) 反應溫度。(10%)

   (4) 氧氣之添加量。(10%)

2. 上述參數對於二硝基甲苯降解之影響力排序爲何？ (10%)

二. 根據附件二，回答下列問題：

1. 本篇論文的研究目的？ (10%)

2. 請說明文中針對 GG mats 所使用的三種架橋方法之條件？(10%)

3. 請說明不同架橋方法對 GG mats 在水中穩定性的影響，並說明其關鍵因素爲何？(15%)

4. 本篇論文有何具體貢獻？ (15%)

Journal of Hazardous Materials 169 (2009) 868–874

Contents lists available at ScienceDirect

Journal of Hazardous Materials

journal homepage: www.elsevier.com/locate/jhazmat

Sonochemical decomposition of dinitrotoluenes and trinitrotoluene in wastewater

ARTICLE INFO

Article history:
Received 16 December 2008
Received in revised form 7 April 2009
Accepted 7 April 2009
Available online 15 April 2009

Keywords:
Pyrolysis
Dinitrotoluene
2,4,6-Trinitrotoluene
Ultrasonic irradiation

ABSTRACT

Mineralization of dinitrotoluenes (DNT) and 2,4,6-trinitrotoluene (TNT) in wastewater was conducted under ultrasonic irradiation. The batch-wise experiments were carried out to elucidate the influence of various operating parameters on the sonolytic behavior, including power intensity, acidity of wastewater, reaction temperature and oxygen dosage. It is remarkable that the nitrotoluenes contained could be almost completely decomposed by the sonochemical oxidation method, wherein the pyrolytic reaction was responsible for the destruction of organic compounds. During the sonication tests, the influence of reaction temperature on the degradation of nitrotoluenes is the most significant, followed by power intensity, acidity of wastewater and oxygen dosage. Based on the spectra obtained from gas chromatograph/mass spectrometer (GC/MS), it is suggested that 2,4,6-TNT is preliminarily denitrated to 2,6-DNT. The denitration of 2,6-DNT and/or 2,4-DNT results in the formation of *o*-mononitrotoluene, which proceeds with the cleavage of nitro group into toluene, followed by oxidation of methyl group and decarboxylation. In this study, it is believed that the sonolytic technique established is promising for wastewater disposal in toluene nitration processes.

1. Introduction

Toluene nitration processes have been well developed due to the industrial importance of dinitrotoluene (DNT) and 2,4,6-trinitrotoluene (TNT), which are precursors of dyes, paints, synthetic leather and explosives, respectively [1]. Traditionally, the aromatics nitration reaction is conducted using nitrating acid, consisting of a mixture of nitric acid and concentrated sulfuric acid. In the preliminary course of separating section, the nitrotoluene product decanted from the settler would be violently blended with alkaline aqueous solution to partially neutralize entrained sulfuric and nitric acids. Subsequently, the residual contaminants in nitrotoluenes were removed by virtue of clean water washing twice, which constitutes the bulk of wastewater upon combination with the above aqueous stream. Because of the toxicity and resistance to biodegradation caused by DNT isomers and TNT derivatives [2,3], the wastewater from toluene nitration processes should be properly treated prior to release into the environment.

Until now, the oxidative degradation of nitrotoluenes in wastewater has attracted much attention. Based on the results of the literatures [4–6], TiO_2 has been proved to be highly effective in photocatalytic degradation of 2,4,6-TNT, wherein the degradation pathways were also elucidated. In addition, Li et al. [7,8] investigated the destruction of 2,4,6-TNT by Fenton's reagent, of which reactivity was enhanced at pH 3.0. In other respect, several studies have focused on the mineralization of nitroaromatic compounds by UV/Fenton's reagent [9,10] or UV/H_2O_2 technique [11,12]. Some publications have been issued on the decomposition of 2,6-DNT using ozonation, H_2O_2/O_3 or UV/O_3 methods [13,14]. In our previous studies [15,16], it has been shown that most of DNTs and 2,4,6-TNT could be recovered from wastewater by means of toluene extraction, wherein the recovery efficiency of nitrotoluenes was significantly enhanced with either increasing acidity of wastewater (pH 3.0) or addition of inorganic salts, whose promoting effect is in the following order: NaCl > Na_2SO_4 > K_2SO_4 > $MgSO_4$ > KCl on the weight basis of wastewater.

It has been recognized that ultrasonic irradiation brings about the formation and collapse of tiny gas bubbles in water. In the course of collapse, local reaction sites of several thousand degrees and several hundred atmospheres are generated due to the quasi-adiabatic procedure, which is known as cavitation [17,18]. During the cavitation, the degradation of pollutants proceeds either via the hydroxyl radicals reaction in the bulk liquid solution, and/or via a direct pyrolysis reaction in the collapsing hot bubbles and at the interface of the gas–liquid [19]. To date, sonochemical oxidation technology has been successfully used for treatment of hazardous organic compounds in wastewater, such as carbon tetrachloride [20], aniline [21], phenol and derivatives [22–28], chlorobenzene

* Corresponding author. Tel.: +886 5 534 2601x4624; fax: +886 5 531 2071.
E-mail address: chenwen@yuntech.edu.tw (W.-S. Chen).

0304-3894/$ – see front matter © 2009 Elsevier B.V. All rights reserved.
doi:10.1016/j.jhazmat.2009.04.028

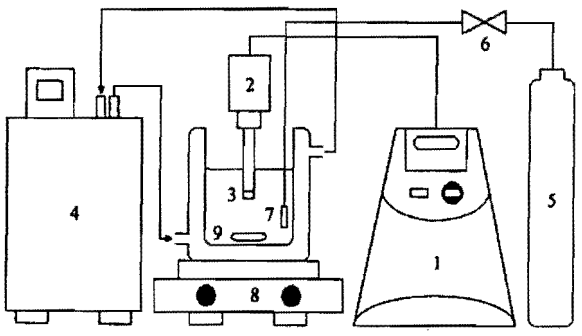

1. Ultrasound Generator
2. Transducer
3. Tip
4. Thermostat
5. Oxygen Gas
6. Mass Flow Meter
7. Oxygen Pipe Diffuser
8. Magnetic Stirrer
9. Stirring Bar

Fig. 1. Schematic illustration of the experimental apparatus for sonication tests. (1) Ultrasound generator, (2) transducer, (3) tip, (4) thermostat, (5) oxygen gas, (6) mass flow meter, (7) oxygen pipe diffuser, (8) magnetic stirrer, and (9) stirring bar.

[29], nitrobenzene and *p*-nitrotoluene [30,31], whereas the sonochemical degradation of DNTs and 2,4,6-TNT from toluene nitration process was scarcely discussed. Consequently, the purpose of this research investigates the feasibility of destruction of nitrotoluenes in industrial wastewater utilizing ultrasonic irradiation. The influences of power intensity, reaction temperature, acidity of wastewater and oxygen dosage on the removal efficiency of nitrotoluenes were elucidated simultaneously. Besides, the sonochemical degradation pathways of DNTs and 2,4,6-TNT were also explored.

2. Experimental

2.1. Sonication testing

Fig. 1 presents the schematic illustration of the experimental apparatus. Ultrasonic irradiation was supplied by an ultrasonic generator (Misonix S-3000 Model, 600 W output, variable power control), which was coupled with a 20 kHz transducer (Φ 40 mm × 120 mm) and a titanium probe (Φ 13 mm × 60 mm). The reaction vessel was a double jacket cylinder (PIIN JIA Technology Co., JC-A16 Model) equipped with a magnetic stirrer (Heidolph MR 3001K Model), which was sealed in a stainless box during operation. Prior to tests, proportionate amount of industrial wastewater (300 mL, rendered by military ammunition plant) was situated in the reactor, wherein the temperature of wastewater was maintained at 298 ± 0.5 K using a thermostat (VWR Scientific Co., 1167 Model) fitted with a circulating water bath. The transducer was fixed through the center of the stainless box and the probe was partially immersed in the wastewater. In the course of sonication tests, oxygen gas monitored by the mass flow meter (BROOKS 5850E Model) was introduced into the wastewater through a porous pipe-diffuser. In this research, the experiments were carried out in a batch-wise mode with various ultrasonic power intensity of 52 W cm^{-2}, 102 W cm^{-2} and 227 W cm^{-2} (as quoted by the manufacturer). At the different duration of irradiation time, the wastewater was periodically sampled from the reactor and undergone total organic compounds (TOC) analyses to evaluate the residual organic compound contents.

In order to investigate the influence of reaction temperature on the removal of nitrotoluenes, three tests with various reaction temperature (298 K up to 328 K) were carried out. Additionally, for the purpose of exploring the effect of oxygen dosage on the destruction of nitrotoluenes, a series of tests with oxygen flow rate of 50 mL min^{-1} up to 200 mL min^{-1} were conducted. The sonication tests were also performed at the pH values of 0.1 up to 1.5 to elucidate the influence of acidity of wastewater on the decomposition of nitrotoluenes.

2.2. Total organic compounds (TOC) analysis

For the duration of sonication tests, the wastewater was periodically analyzed using a TOC instrument (Tekmar Dohrmann Phoenix 8000 Model) equipped with an ultra-violet (UV) reactor and a nondispersive infrared (NDIR) detector. The organic compounds in wastewater were completely oxidized into carbon dioxide by sodium persulfate assisted with UV irradiation, which was subsequently quantified by the NDIR detector. In contrast, the inorganic compounds acidified by phosphoric acid were removed in advance by way of carbonic acid. The samples were directly analyzed without further treatment to meet the measuring ranges (0–200 mg L^{-1}), calibrated by the potassium hydrogen phthalate standard solution.

2.3. Gas chromatograph/mass spectrometer (GC/MS) analysis

As sonication testing was performed for 2 h, the wastewater sampled (ca. 50 mL) was blended with equivalent volume of dichloromethane (≥99.5%, Fluka) in an extractor to extract and concentrate the degradation intermediates involved, as described in detail in a previous report [32]. Subsequently, the dichloromethane extract was analyzed using a gas chromatograph/mass spectrometer (Hewlett Packard 59864B/HP 5973 MASS) equipped with a capillary column (Metal ULTRA ALLOY UA-5, 30 m × 0.25 mm, film thickness 0.25 μm), programming from 313 K to 573 K at an elevation rate of 20 K min^{-1} and maintaining the temperature at 573 K for 1 h. The mass spectra of degradation intermediates were identified by comparing with those of the authentic standard compounds in database (Wiley 275L).

2.4. Hydrogen peroxide concentration analysis

The concentration of hydrogen peroxide generated in the deionized water (pH 0.1) with the presence of oxygen gas by ultrasonic irradiation was determined by the titanic sulfate method, wherein the light absorbance of titanic–hydrogen peroxide was measured using an UV–vis spectrophotometer (LAMBDA 850 Model, PerkinElmer) at a wavelength of 410 nm [33]. The sample (ca. 4 mL) was situated in a quartz holder and directly analyzed to meet the measuring limit requirement of 0–50 mg L^{-1}, corrected by the standard solution of hydrogen peroxide.

2.5. Adjustment of pH value of wastewater

The experiments were conducted in a hot plate (Heidolph MR 3001K Model) accompanied with magnetic agitation (ca. 400 rpm). The wastewater (300 mL) was situated in the jacket beaker, wherein the solution temperature was maintained at 303 K by a thermostat (VWR Scientific Co., 1167 Model) equipped with a circulating water bath. On addition of appropriate amounts of sodium hydroxide solution (0.1 mol L^{-1}), the acidity of wastewater was adjusted to the pH values of 0.5, 1.0 and 1.5, respectively (measured by SUNTEX SP-701 PH/mV/TEMP Meter).

Table 1
Compositions of TOC feedstock and reaction intermediates in wastewater identified by GC/MS.

Component	m/z (relative abundance, %)
TOC feedstock	
2,6-DNT	63 (36.1), 77 (20.1), 78 (16.9), 89 (40.8), 90 (27.5), 121 (17.9), 148 (21.5), 165 (100)
2,4-DNT	51 (13.2), 63 (36.1), 64 (13.4), 78 (16.8), 89 (60.9), 90 (26.3), 119 (26.0), 165 (100)
3,4-DNT	30 (64.7), 39 (32.9), 52 (33.0), 63 (47.5), 66 (33.2), 78 (46.6), 89 (51.5), 182 (100)
2,4,6-TNT	30 (15.1), 62 (16.5), 63 (32.5), 76 (15.1), 89 (43.4), 180 (14.0), 193 (13.6), 210 (100)
Reaction intermediates	
Toluene	39 (8.2), 51 (5.3), 63 (7.1), 65 (11.0), 89 (4.4), 91 (100), 92 (59.9), 93 (4.6)
o-MNT	39 (28.3), 63 (28.0), 65 (83.3), 77 (30.6), 89 (30.7), 91 (60.9), 92 (62.4), 120 (100)
Benzoic acid	39 (7.5), 50 (24.9), 51 (40.2), 74 (10.2), 77 (76.9), 78 (8.1), 105 (100), 122 (79.0)
2,6-DNT	63 (36.1), 77 (19.9), 78 (16.8), 89 (40.5), 90 (27.4), 121 (17.8), 148 (21.2), 165 (100)
2,4-DNT	51 (13.3), 63 (36.0), 64 (13.2), 78 (16.7), 89 (60.9), 90 (26.3), 119 (25.9), 165 (100)
3,4-DNT	30 (64.6), 39 (32.8), 52 (32.9), 63 (47.4), 66 (33.1), 78 (46.7), 89 (51.4), 182 (100)
2,4,6-TNT	30 (14.9), 62 (16.6), 63 (32.3), 76 (15.0), 89 (43.3), 180 (13.9), 193 (13.6), 210 (100)

2.6. Statistics analysis

The experiment data was analyzed through a factorial design analysis, wherein the operating parameters, such as power intensity, acidity of wastewater, reaction temperature and oxygen dosage, were taken into consideration. The statistical package of ANOVA (DESIGN-EASE) was used for all analyses. The operating parameter with Model *P*-value <0.0005 is thought to indicate statistical significance. Furthermore, the larger Model *F*-value implies that the operating parameter is more significant.

3. Results and discussion

3.1. Effect of power intensity on sonication

Based on the analysis of GC/MS, the typical components of nitrotoluenes in industrial wastewater from toluene nitration process have been identified as 2,6-DNT, 2,4-DNT, 3,4-DNT and 2,4,6-TNT (Table 1), wherein the concentration of TOC was about 150 mg L^{-1}. The power intensity has been well recognized to be an important operating variable for sonochemical engineering. Fig. 2 demonstrates the time pattern of TOC removal percentage as a function of power intensity. From the figure, it can be seen that the destruction rate of nitrotoluenes increases proportionately with an increase in power intensity, reaches a maximum at about 102 W cm^{-2} and then decreases upon increasing the intensity further. The observation could be interpreted with a significant increase in number of bubbles, close to the emitting surface, caused by sharply increasing the power intensity. The considerable amount of bubbles may coalesce to form large bubbles, which would cavitate less violently than that of tiny bubbles. Therefore, it may lead to lower energy efficiency and formation of fewer amounts of free radicals at the power intensity of 227 W cm^{-2}, in agreement with the report by Sivakumar et al. [34,35]. As a consequence, the optimal power intensity of 102 W cm^{-2} has been chosen for subsequent sonication tests.

3.2. Effect of acidity of wastewater on sonication

For the sake of increasing destruction rate of nitrotoluenes, the adjustment of acidity of wastewater has been always adopted practically. Fig. 3 presents the influence of acidity of wastewater on the ultrasonic degradation of TOC. Obviously, the nitrotoluene removal efficiency exhibits an increasing trend with increasing the acidity of wastewater. According to our earlier work [15], the extraction efficiency of DNTs and 2,4,6-TNT from wastewater by toluene solvent would be significantly enhanced with a reduce of pH values. It means that the stronger hydrophobicity of DNTs and 2,4,6-TNT is achieved with an increase of acidity of wastewater, leading to a great many of nitrotoluenes concentrated at the gas–liquid interface of the bubbles [19,36]. Nonetheless, it has been suggested that

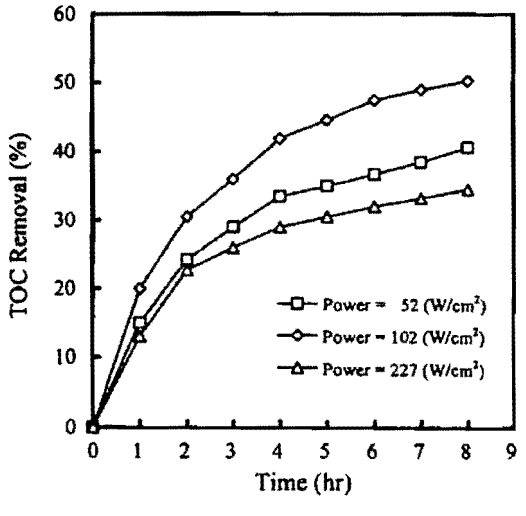

Fig. 2. Effect of power intensity on the mineralization of TOC in wastewater under the conditions of T = 298 K, O_2 = 0 mL min^{-1} and pH 0.1 for sonication tests.

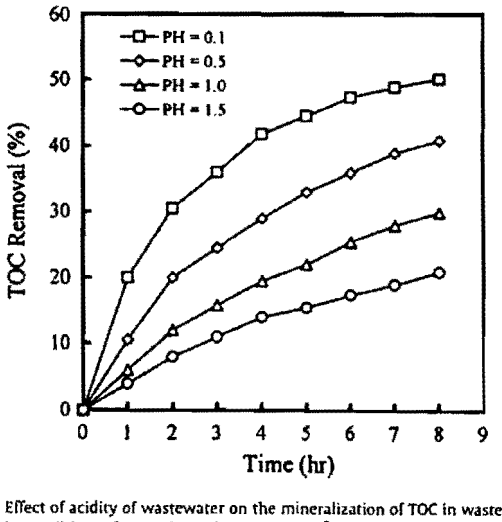

Fig. 3. Effect of acidity of wastewater on the mineralization of TOC in wastewater under the conditions of power intensity = 102 W cm^{-2}, T = 298 K and O_2 = 0 mL min^{-1} for sonication tests.

附件一

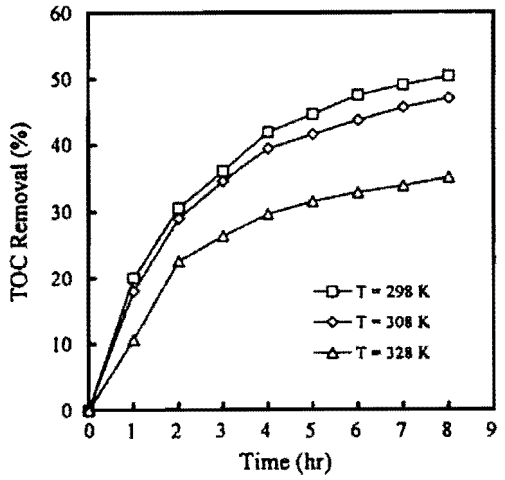

Fig. 4. Effect of reaction temperature on the mineralization of TOC in wastewater under the conditions of power intensity = 102 W cm^{-2}, pH 0.1 and O_2 = 0 mL min^{-1} for sonication tests.

there are two main degradation pathways for the sonochemical oxidation of organic compounds in aqueous solution. One is the pyrolytic reactions that occur in the hot cavitation bubbles and/or at the gas–liquid interface of the bubbles. The other is the reactions involving hydroxyl radicals at the gas–liquid interface of the bubbles and in the bulk liquid [37]. Besides, the result corresponds to the publication by Chakinala et al. [38] for the sonochemical destruction of hydrophobic compound of salicylic acid enhanced with acidic conditions.

3.3. Effect of reaction temperature on sonication

Based on the industrial process design of sonochemical oxidation technology, it is essential to determine the appropriate reaction temperature, at which higher destruction efficiency of organic compounds was achieved. Fig. 4 illustrates the time pattern of TOC removal percentage as a function of reaction temperature. Apparently, the TOC removal efficiency at 298 K was higher than that at 308 K. In fact, an identical trend was also found as compared the data of 308 K with that of 328 K. It seems that the lower reaction temperature is in favor of sonochemical degradation of TOC. This phenomenon may be interpreted with the decrease in cavitation intensity resulted from an increase of solvent vapor pressure due to the elevation of reaction temperature, in coincidence with the research by Goskonda et al. [39]. Furthermore, the result implies that the cavitation plays an important role on the sonochemical decomposition of DNTs and 2,4,6-TNT, including pyrolytic reactions and production of free radicals.

3.4. Effect of dosage of oxygen on sonication

For the purpose of enhancing destruction efficiency of nitrotoluenes, the wastewater was dosed with oxygen gas, which speeds up the initialization of cavity formation via provision of excess nuclei [40]. Fig. 5(a) presents the influence of flow rate of oxygen on the sonolytic behavior. It clearly shows that the destruction rate of TOC increases significantly with an increase of oxygen flow rate. Besides, it is remarkable that the nitrotoluenes in wastewater could be almost completely decomposed under the conditions of power intensity = 102 W cm^{-2}, T = 298 K, pH 0.1 and O_2 = 200 mL min^{-1}. The observation may be partially ascribed to the generation of hydroxyl radicals, resulted from dissociation of molecular oxygen in

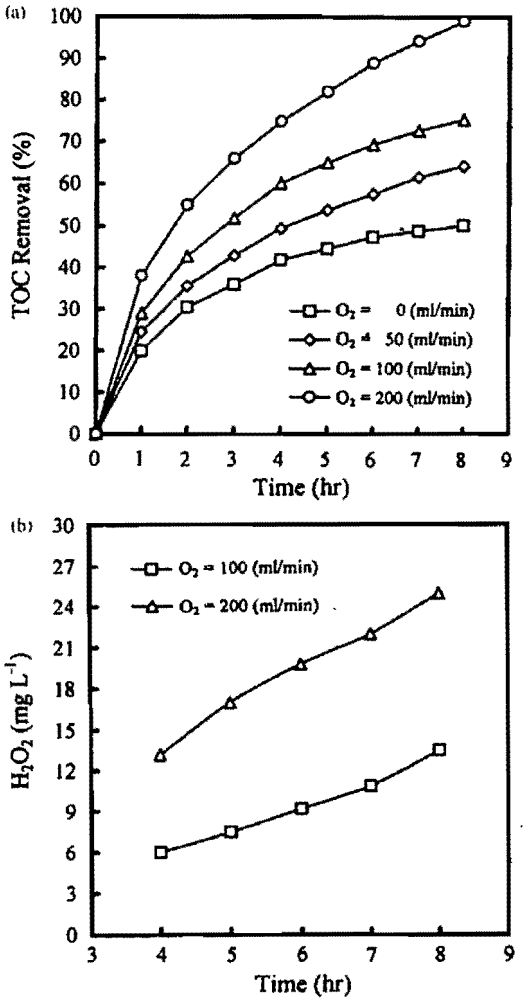

Fig. 5. (a) Effect of oxygen dosage on the mineralization of TOC in wastewater under the conditions of power intensity = 102 W cm^{-2}, T = 298 K and pH 0.1 for sonication tests. (b) Time pattern of hydrogen peroxide concentration accumulated in deionized water under the conditions of power intensity = 102 W cm^{-2}, T = 298 K and pH 0.1 during sonication tests.

the bubble, which is likely to recombine to form hydrogen peroxide at the gas–liquid interface of the bubbles [41]:

$$O_2 \rightarrow 2O^{\bullet} \quad (1)$$

$$O^{\bullet} + H_2O \rightarrow 2HO^{\bullet} \quad (2)$$

$$2HO^{\bullet} \rightarrow H_2O_2 \quad (3)$$

In order to verify the generation of hydrogen peroxide, which has been proved to be effective for decomposition of DNTs and 2,4,6-TNT previously [42], the sonication tests in the absence of nitrotoluenes were carried out. As shown in Fig. 5(b), the hydrogen peroxide concentration accumulated in deionized water (pH 0.1) increases with an increase of oxygen dosage. The yield of hydrogen peroxide reaches to a value as high as 25 mg L^{-1} under sonication for 8 h, whereas it could only abate some nitrotoluenes in comparison with the total amounts of nitrotoluenes removed (150 mg L^{-1}). Consequently, it reveals that the DNTs and 2,4,6-TNT in wastewater were principally destructed by way of pyrolytic reaction, deduced from the cavitation. Additionally, the result convinces us that the

國立雲林科技大學
101 學年度博士班招生考試試題

所別：化學工程與材料工程系
科目：科技文獻

附件一

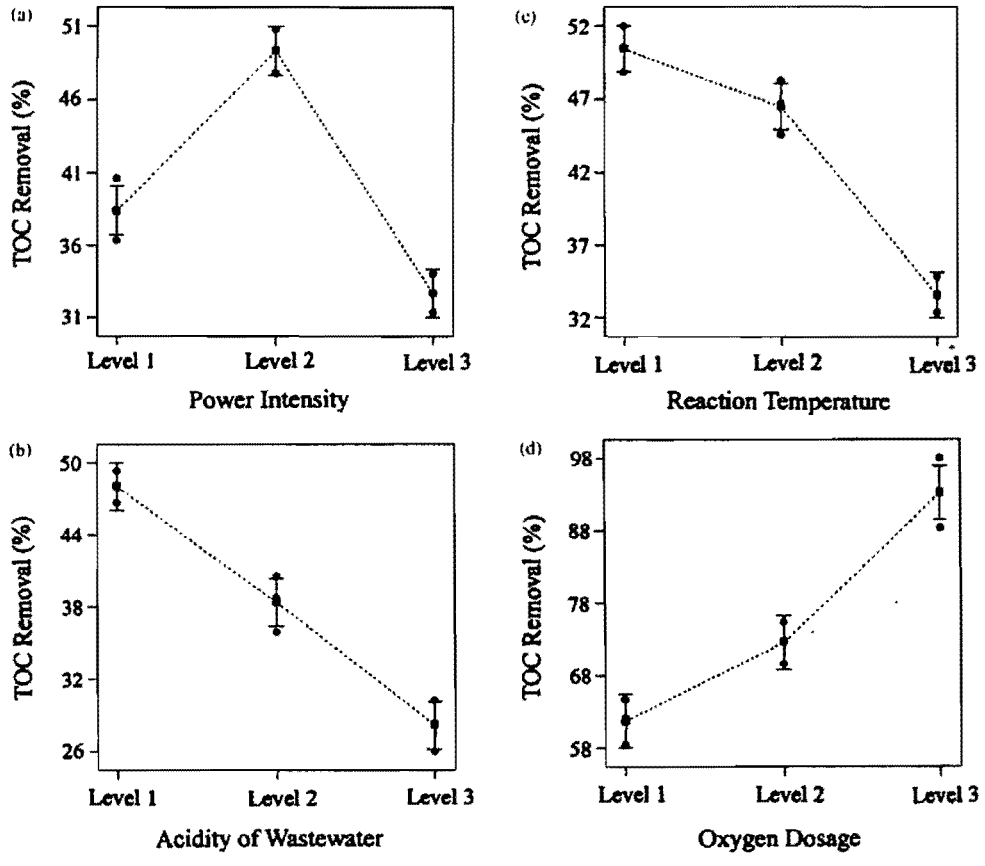

Fig. 6. Factorial design analyses of four operating variables on the sonochemical oxidation of nitrotoluenes (a) power intensity, (b) acidity of wastewater, (c) reaction temperature, and (d) oxygen dosage.

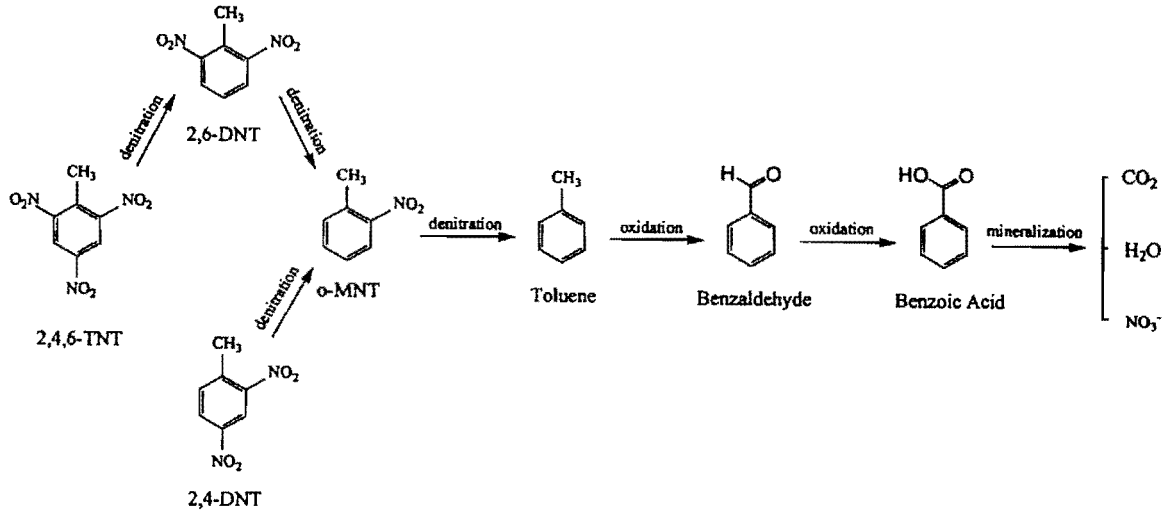

Fig. 7. Plausible reaction pathways of DNTs and 2,4,6-TNT in wastewater under ultrasonic irradiation.

sonochemical oxidation technology is suitable for direct disposal of industrial wastewater from toluene nitration processes.

3.5. Examination of the significance of operating variables

It is very important to explore the influence of operating parameters individually on the sonolytic behavior for development of a new process. Consequently, a factorial design analysis (ANOVA Model, DESIGN-EASE) was carried out in dealing with four factors, i.e. power intensity, acidity of wastewater, reaction temperature and oxygen dosage, using three levels (shown as Fig. 6). On the basis of statistical analyses of the data in these plots, it was found that the Model *F*-value for power intensity, acidity of wastewater, reaction temperature and oxygen dosage were 76, 74, 95 and 56, respectively, wherein the Model *P*-value were all less than 0.0001. That implies the influence of reaction temperature on the sonochemical oxidation of nitrotoluenes is the most significant, followed to a decreasing extent by power intensity, acidity of wastewater and oxygen dosage.

3.6. Reaction pathways of nitrotoluenes by sonication

In order to elucidate the degradation intermediates involved in sonochemical oxidation of DNTs and 2,4,6-TNT, the dichloromethane extract was analyzed using a GC/MS spectrometer. Table 1 summarizes the results, wherein the compositions consist of toluene, *o*-mononitrotoluene (MNT), benzoic acid, 2,6-DNT, 2,4-DNT, 3,4-DNT and 2,4,6-TNT. With regard to the components of 2,6-DNT, 2,4-DNT, 3,4-DNT and 2,4,6-TNT, they may be attributed to the nitrotoluene feedstock in wastewater. Nevertheless, in nitrotoluene feedstock there was not any MNT detected, which has been proved to be decomposed faster than DNTs and TNT by hydroxyl radicals [9]. As a consequence, the *o*-MNT could be proposed as one of reaction intermediates during sonication testing. It is believed that *o*-MNT is derived from 2,4-DNT and/or 2,6-DNT, wherein the electron-donating methyl group would elevate the electron density of nitro groups to be oxidized more easily [43]. The nitro group of *o*-MNT was subsequently cleaved from benzene ring for the same reason as described, which is also consistent with the report by Kotronarou et al. [44], who has suggested that the preliminary reaction pathway was carbon–nitrogen bond cleavage during the sonochemical oxidation of *p*-nitrophenol. Eventually, toluene would be further oxidized to benzaldehyde, followed with decarboxylation of benzoic acid and the mineralization step gave rise to the ultimate products of carbon dioxide, nitrate ions and water.

As regards the degradation pathway of 2,4,6-TNT, it is likely that 2,4,6-TNT was firstly denitrated to 2,6-DNT based on the same reaction mechanism as mentioned, wherein the *p*-nitro group was preferred to be cleaved from benzene ring. Then it would proceed with an identical reaction pathway as that of 2,6-DNT. To sum up, the plausible degradation pathways of DNTs and 2,4,6-TNT under ultrasonic irradiation could be demonstrated in Fig. 7.

4. Conclusions

Based on the previous discussion, it is evident that the DNTs and 2,4,6-TNT in wastewater could be mineralized by pyrolysis, free radicals and hydrogen peroxide, which would be in situ generated via dissociation of oxygen gas. Besides, it is worthy to note that the nearly complete destruction of TOC can be achieved under the optimal conditions of power intensity = 102 W cm^{-2}, T = 298 K, pH 0.1 and O_2 = 200 mL min^{-1}. That means the sonochemical oxidation technique may be directly utilized to treat wastewater practically. With respect to the effect of operating variables on the sonolytic behavior, the reaction temperature is the most significant, followed by power intensity, acidity of wastewater and oxygen dosage. According to the spectra given by GC/MS spectrometer, the plausible degradation pathways of nitrotoluenes under ultrasonic irradiation are proposed as follows. At first, 2,4,6-TNT is denitrated to 2,6-DNT. The denitration of 2,6-DNT and/or 2,4-DNT gives rise to *o*-MNT, of which nitro group is successively cleaved to form toluene. Then, the methyl group of toluene is oxidized, followed with the decarboxylation of benzoic acid. Finally, the mineralization procedure leads to ultimate products of carbon dioxide, nitrate ions and water.

Acknowledgement

Financial supports of this work by the National Science Council (Grant No. NSC 96-2221-E-224-017-MY2) are gratefully acknowledged.

References

[1] Ullmann's Encyclopedia of Industrial Chemistry, vol. A17, fifth ed., VCH, Weinheim, 1991, p. 411.
[2] W.D. Won, L.H. Di Salvo, J. Ng, Toxicity and mutagenicity of 2,4,6-trinitrotoluene and its metabolites, Appl. Environ. Microbiol. 31 (1976) 576–580.
[3] P.B. Tchounwou, B.A. Wilson, A.B. Ishaque, J. Schneider, Transcriptional activation of stress genes and cytotoxicity in human liver carcinoma cells ($HepG_2$) exposed to 2,4,6-trinitrotoluene, 2,4-dinitrotoluene, and 2,6-dinitrotoluene, Environ. Toxicol. 16 (2001) 209–216.
[4] D.C. Schmelling, K.A. Gray, Photocatalytic transformation and mineralization of 2,4,6-trinitrotoluene (TNT) in TiO_2 slurries, Water Res. 29 (1995) 2651–2662.
[5] R. Dillert, M. Brandt, I. Fornefett, U. Siebers, D. Bahnemann, Photocatalytic degradation of trinitrotoluene and other nitroaromatic compounds, Chemosphere 30 (1995) 2333–2341.
[6] M.S. Vohra, K. Tanaka, Photocatalytic degradation of trinitrotoluene in aqueous TiO_2 suspension, Water Res. 36 (2002) 59–64.
[7] Z.M. Li, M.M. Peterson, S.D. Comfort, G.L. Horst, P.J. Shea, B.T. Oh, Remediating TNT-contaminated soil by soil washing and Fenton oxidation, Sci. Total Environ. 204 (1997) 107–115.
[8] Z.M. Li, S.D. Comfort, P.J. Shea, Destruction of 2,4,6-trinitrotoluene by Fenton oxidation, J. Environ. Qual. 26 (1997) 480–487.
[9] Z.M. Li, P.J. Shea, S.D. Comfort, Nitrotoluene destruction by UV-catalyzed Fenton oxidation, Chemosphere 36 (1998) 1849–1865.
[10] M.-J. Liou, M.-C. Lu, J.-N. Ohen, Oxidation of explosives by Fenton and photo-Fenton process, Water Res. 37 (2003) 3172–3179.
[11] P.C. Ho, Photooxidation of 2,4-dinitrotoluene in aqueous solution in the presence of hydrogen peroxide, Environ. Sci. Technol. 20 (1986) 260–267.
[12] S. Hwang, E.J. Bouwer, S.L. Larson, J.L. Davis, Decolorization of alkaline TNT hydrolysis effluents using UV/H_2O_2, J. Hazard. Mater. 108 (2004) 61–67.
[13] F.J. Beltrán, J.M. Encinar, M.A. Alonso, Nitroaromatic hydrocarbon ozonation in water. 1. Single ozonation, Ind. Eng. Chem. Res. 37 (1998) 25–31.
[14] F.J. Beltrán, J.M. Encinar, M.A. Alonso, Nitroaromatic hydrocarbon ozonation in water. 2. Combined ozonation with hydrogen peroxide or UV radiation, Ind. Eng. Chem. Res. 37 (1998) 32–40.
[15] W.S. Chen, W.C. Chiang, C.C. Lai, Recovery of nitrotoluenes in wastewater by solvent extraction, J. Hazard. Mater. 145 (2007) 23–29.
[16] W.S. Chen, W.C. Chiang, K.M. Wei, Recovery of nitrotoluenes from wastewater by solvent extraction enhanced with salting-out effect, J. Hazard. Mater. 147 (2007) 197–204.
[17] W.B. McNamara III, Y.T. Didenko, K.S. Suslick, Pressure during sonoluminescence, J. Phys. Chem. B 107 (2003) 7303–7306.
[18] K. Okitsu, T. Suzuki, N. Takenaka, H. Bandow, R. Nishimura, Y. Maeda, Acoustic multibubble cavitation in water: a new aspect of the effect of a rare gas atmosphere on bubble temperature and its relevance to sonochemistry, J. Phys. Chem. B 110 (2006) 20081–20084.
[19] B. Nanzai, K. Okitsu, N. Takenaka, H. Bandow, Y. Maeda, Sonochemical degradation of various monocyclic aromatic compounds: relation between hydrophobicities of organic compounds and the decomposition rates, Ultrason. Sonochem. 15 (2008) 478–483.
[20] C. Pétrier, A. Francony, Ultrasonic waste-water treatment: incidence of ultrasonic frequency on the rate of phenol and carbon tetrachloride degradation, Ultrason. Sonochem. 4 (1997) 295–300.
[21] S. Song, Z.Q. He, J.M. Chen, US/O_3 combination degradation of aniline in aqueous solution, Ultrason. Sonochem. 14 (2007) 84–88.
[22] R. Kidak, N.H. Ince, Ultrasonic destruction of phenol and substituted phenols: a review of current research, Ultrason. Sonochem. 13 (2006) 195–199.
[23] P.S. Bapat, P.R. Gogate, A.B. Pandit, Theoretical analysis of sonochemical degradation of phenol and its chloroderivatives, Ultrason. Sonochem. 15 (2008) 564–570.
[24] I. Gültekin, N.H. Ince, Ultrasonic destruction of bisphenol-A: the operating parameters, Ultrason. Sonochem. 15 (2008) 524–529.

Acta Biomaterialia 7 (2011) 1702–1709

Contents lists available at ScienceDirect

Acta Biomaterialia

journal homepage: www.elsevier.com/locate/actabiomat

Electrospun gelatin nanofibers: Optimization of genipin cross-linking to preserve fiber morphology after exposure to water

Silvia Panzavolta [a], Michela Gioffrè [a], Maria Letizia Focarete [a], Chiara Gualandi [a], Laura Foroni [b], Adriana Bigi [a,*]

[a] Department of Chemistry "G. Ciamician" and National Consortium of Materials Science and Technology (INSTM, Bologna RU), University of Bologna, Via Selmi 2, 40126 Bologna, Italy
[b] Department of Specialistic Surgical and Anaesthesiological Sciences, University of Bologna, Via Massarenti 9, 40138 Bologna, Italy

ARTICLE INFO

Article history:
Received 25 August 2010
Received in revised form 8 November 2010
Accepted 17 November 2010
Available online 21 November 2010

Keywords:
Scaffold
Gelatin
Electrospinning
Genipin
Cross-linking

ABSTRACT

The development of suitable biomimetic three-dimensional scaffolds is a fundamental requirement of tissue engineering. This paper presents the first successful attempt to obtain electrospun gelatin nanofibers cross-linked with a low toxicity agent, genipin, and able to retain the original nanofiber morphology after water exposure. The optimized procedure involves an electrospinning solution containing 30 wt.% gelatin in 60/40 acetic acid/water (v/v) and a small amount of genipin, followed by further cross-linking of the as-electrospun mats in 5% genipin solution for 7 days, rinsing in phosphate-buffered saline and then air drying at 37 °C. The results of scanning electron microscopy investigations indicated that the cross-linked nanofibers were defect free and very regular and they also maintained the original morphology after exposure to water. Genipin addition to the electrospinning solution dramatically reduced the extensibility of the as-electrospun mats, which displayed further remarkable improvements in elastic modulus and stress at break after successive cross-linking up to values of about 990 and 21 MPa, respectively. The results of the preliminary in vitro tests carried out using vascular wall mesenchymal stem cells indicated good cell viability and adhesion to the gelatin scaffolds.

1. Introduction

A suitable three-dimensional porous bioresorbable scaffold is considered mandatory for the successful development of an engineered tissue as a biological substitute. To this end, the scaffold should display structural and chemical properties matching as far as possible those of the extracellular matrix (ECM) [1–3].

Electrospinning is a simple and cost-effective technique that allows the fabrication of scaffolds, from both synthetic and natural polymers, mimicking the three-dimensional nano-scaled features of the ECM [4]. Synthetic bioresorbable polymers provide structural functionalities to the scaffold. On the other hand, natural polymers display unique bioactive properties and excellent cellular affinity.

Collagen type I, the most abundant structural protein in the human body, has frequently been used to produce electrospun scaffolds [5–8]. Compared with collagen, gelatin, which can be obtained through collagen thermal denaturation or physical and chemical degradation, is cheaper and does not show antigenicity under physiological conditions [9,10]. Moreover, gelatin is biodegradable, biocompatible and displays many integrin binding sites for cell adhesion and differentiation. For these reasons gelatin is widely used in the pharmaceutical and medical fields in a variety of applications, including tissue engineering, wound dressing, drug delivery and gene therapy [11].

Although gelatin has been successfully electrospun into ultrafine fibers, the preparation of gelatin scaffolds by means of electrospinning raises some critical issues. First, highly toxic solvents, among which are 1,1,1,3,3,3-hexaflouro-2-propanol [12] and 2,2,2-trifluoroethanol [9,13], are typically used to dissolve the protein. Acetic acid [14], as well as water mixtures with acetic acid and ethyl acetate [15], have been proposed as solvents to circumvent this problem. The solubility of the as-spun gelatin fibers is a further drawback for long-term medical applications. Cross-linking, which is necessary to improve the water resistance of the nanofibers, introduces an additional major issue when gelatin is used to create tissue engineered scaffolds. Indeed, cross-linking treatment of these materials must not only prevent gelatin dissolution in water but also preserve the peculiar biomimetic nanofibrous morphology of the electrospun scaffolds.

Collagenous materials can be cross-linked using either physical methods, such as dehydrothermal treatment and ultraviolet and gamma irradiation, or chemical agents. Chemical cross-linking exploits the large number of functional gelatin side groups and usually involves bifunctional reagents such as glutaraldehyde and diisocyanates, as well as genipin, carbodiimides, acyl azide and polyepoxy compounds [10,16–18]. Cross-linking with glutaralde-

* Corresponding author. Tel.: +39 051 2099551; fax: +39 051 2099456.
E-mail address: adriana.bigi@unibo.it (A. Bigi).

1742-7061/$ - see front matter © 2010 Acta Materialia Inc. Published by Elsevier Ltd. All rights reserved.
doi:10.1016/j.actbio.2010.11.021

hyde vapors is a simple, low cost, effective method to stabilize collagenous and gelatin-based materials that has successfully been applied to electrospun gelatin fibers [9,19]. However, if released into the host due to biodegradation, glutaraldehyde is toxic [20]. Among the alternative cross-linking agents genipin has been reported to provide materials with higher biocompatibility and less cytotoxicity [21,22]. This naturally occurring cross-linking agent, which can be obtained from an iridoid glucoside geniposide) abundant in gardenia fruits, has been successfully applied to both collagenous tissues and gelatin materials [10,23].

Recently genipin was investigated as cross-linking agent for electrospun gelatin [19,24,25]. However, up to now genipin cross-linking procedures applied to gelatin have been unable to maintain the fiber morphology of the electrospun scaffolds upon water contact [19,25].

In this work we optimized the conditions for cross-linking of electrospun gelatin with genipin in order to stabilize the nanofibers and maintain their morphology even after exposure to an aqueous solution.

2. Materials and methods

2.1. Preparation of the solutions for electrospinning

2.1.1. Electrospun fibers from gelatin solution

Type A gelatin (Italgelatine SpA) from porcine skin was dissolved in 60/40 vol.% acetic acid/double distilled water at a concentration of 30% (w/v). The solution was stirred at 50 °C for 60 min and then electrospun. The electrospun mats obtained from this solution are labeled G.

2.1.2. Electrospun fibers from gelatin–genipin solution

Type A gelatin (Italgelatine SpA) from porcine skin was dissolved in 60/40 vol.% acetic acid/double distilled water at a concentration of 30% (w/v). The solution was stirred at 50 °C for 60 min and then 60 mg of genipin (Wako) dissolved in 0.5 ml of ethanol and 1 ml of 0.75 M phosphate-buffered saline (PBS), pH 7.4, were added to 10 ml of the gelatin solution. About 30 min after genipin addition the mixture was electrospun. The obtained mats are labeled GG.

2.2. Electrospun non-woven mat fabrication

The electrospinning apparatus, made in house, was composed of a high voltage power supply (Spellman SL 50 P 10/CE/230), a syringe pump (KD Scientific 200 series), a glass syringe, a stainless steel blunt-ended needle (inner diameter 0.84 mm) connected to the power supply electrode and a grounded circular copper collector (diameter 5 cm). The polymer solution was dispensed through a Teflon tube to the needle, which was placed vertical to the collecting plate. All the above described solutions were electrospun into non-woven mats using the following conditions: applied voltage 15 kV, needle to collector distance 15 cm, solution flow rate 0.005 ml min^{-1}, at room temperature (RT) and a relative humidity (RH) of 42 ± 3%. Electrospun mats were kept under vacuum over P_2O_5 at RT overnight in order to remove residual solvents. Electrospun mats were fixed to plastic rings (CellCrown™, Scaffdex) before proceeding with the cross-linking treatments.

2.3. Cross-linking methods

The conditions utilized for the different cross-linking methods are summarized in Table 1.

2.3.1. Method A

GG mats were soaked in 5%, 7% or 11% (w/v) genipin solution in ethanol for 7 days, at a temperature of 37 °C. Subsequently the mats were dried overnight at 37 °C, then rinsed in ethanol and dried again. Cross-linked samples were labeled GG_5A, GG_7A and GG_11A.

Table 1
Cross-linking conditions used for the different samples.

Sample	Genipin concentration (w/v) (%)	Cross-linking time (days)	Rinsing in PBS	Drying temperature (°C)
GG_5A	5	7	No	37
GG_7A	7	7	No	37
GG_11A	11	7	No	37
GG_5B	5	7	No	45
GG_5C3d	5	3	Yes	37
G_5C3d	5	3	Yes	37
GG_5C7d	5	7	Yes	37
G_5C7d	5	7	Yes	37

2.3.2. Method B

GG mats were soaked in 5% (w/v) genipin solution in ethanol for 7 days at 37 °C. Subsequently the mats were dried overnight at 45 °C, then rinsed in ethanol and dried again. Cross-linked samples were labeled GG_5B.

2.3.3. Method C

G and GG mats were soaked in 5% (w/v) genipin solution in ethanol for either 3 or 7 days at 37 °C. Subsequently the mats were rinsed in 0.1 M PBS, pH 7.4, dried overnight at 37 °C, then rinsed in ethanol and dried again. Cross-linked samples were labeled GG_5C3d, GG_5C7d, G_5C3d and G_5C7d.

2.4. Films preparation

Gelatin was dissolved in double distilled water at 50 °C for 60 min. Films were obtained on the bottom of Petri dishes (diameter 6 cm) after water evaporation at RT from 10 ml of gelatin solution. Films were prepared from solutions at 30% (w/v) gelatin concentration in double distilled water or in 60/40 vol.% acetic acid/double distilled water. Alternatively, films were obtained from 10 ml of 30% (w/v) gelatin in 60/40 vol.% acetic acid/double distilled water, with the addition of 60 mg of genipin dissolved in 0.5 ml of ethanol and 1 ml of 0.75 M PBS, pH 7.4. Films for Fourier transform infra-red (FTIR) analysis were prepared from the same gelatin solutions as above after dilution at 1:20.

2.5. Characterization

2.5.1. X-ray diffraction analysis

X-ray diffraction analysis was carried out using a Panalytical XCelerator powder diffractometer. CuK_α radiation was used (40 mA, 40 kV). The 2θ range was from 5° to 25° with a step size of 0.1° and a time per step of 700 s.

2.5.2. Infrared absorption analysis

FTIR analysis of electrospun mats and gelatin films was carried out using a Perkin Elmer model 682. The spectra were collected in the range 4000–400 cm^{-1} at a resolution of 4 cm^{-1}.

2.5.3. Morphological investigation

Morphological investigation of the samples was performed using a Philips XL-20 scanning electron microscope. The samples were sputter-coated with gold prior to examination. The distribution of fiber diameters was determined by the measurement of a number of fibers (100–250) using acquisition and image analysis software (EDAX Genesis) and the results are given as the average diameter ± standard deviation.

Single factor analysis of variance (ANOVA) was employed to assess statistical significance of the results. $P < 0.001$ was considered statistically significant.

2.5.4. Cross-linking degree

The extent of cross-linking of gelatin mats was determined by a UV assay of uncross-linked ε-amino groups before and after cross-linking [26]. Following reaction with 0.5% trinitrobenzensulfonic acid (TNBS), gelatin nanofibers were hydrolyzed with 6 M HCl and extracted with ethyl ether. The absorbance of the diluted solution was measured at 346 nm in a Kontron Uvikon 931 spectrophotometer against a blank. The relationship between absorbance and moles of ε-amino groups per gram of gelatin is:

$$\text{moles ε-amino groups/g gelatin} = 2(\text{absorbance})(0.020\ \text{l})/(1.46 \times 10^4\ \text{l mol cm}^{-1})bx$$

where 1.46×10^4 l mol cm^{-1} is the molar absorptivity of TNP-lys, b is the cell path length in cm, and x is the sample weight in g.

2.5.5. Mechanical properties

Stress–strain curves of mats (5 × 20 mm, thickness 0.012–0.017 mm, determined by scanning electron microscopy (SEM)) in the dry state were recorded using an Instron Testing Machine 4465, with a cross-head speed of 0.5 mm min^{-1}, and the Series IX software package. The Young's modulus E, the strain at break ε_b and the stress at break σ_b of the strips were measured in static mode.

Single factor analysis of variance (ANOVA) was employed to assess statistical significance of the results. $P < 0.001$ was considered statistically significant.

2.6. In vitro tests

2.6.1. Cell seeding and culture

Vascular wall mesenchymal stem cells (VW-MSCs), isolated from human femoral arteries as previously reported [27], were used to assess the biocompatibility of G and GG electrospun nanofibrous scaffolds. VW-MSCs were propagated in Dulbecco's modified Eagle's medium (DMEM) containing 4.5 g l^{-1} glucose supplemented with 10% fetal bovine serum (FBS), 2 mM L-glutamine and 100 U ml^{-1} penicillin/streptomycin at 37 °C in 5% CO_2. Before cells seeding G and GG electrospun mats were sterilized by immersion in 85% ethanol for 15 min, then 70% ethanol for 15 min, followed by three rinses with PBS plus 2% penicillin/streptomycin (Euroclone), 0.2% amphotericin B (Sigma). Scaffolds were kept in this solution overnight under UV irradiation (230 V at 50 Hz). The next day the PBS solution was removed and the scaffolds were pre-wetted in complete culture medium. When 80% confluence was reached the cells were trypsinized (0.05% Trysin-EDTA, Sigma), centrifuged and resuspended in medium. Cells were then seeded (2×10^4) onto the scaffolds, which were fixed to plastic rings (CellCrowns™ 12, Scaffdex) and cultured under standard culture conditions (37 °C, 5% CO_2) for 7 days before being processed for SEM analysis.

2.6.2. Cell morphology

After 7 days culture specimens were processed for SEM analysis. Briefly, samples were fixed in 2.5% buffered glutaraldehyde overnight at 4 °C, washed with 0.15 M PBS, pH 7.4, and post-fixed with 1% osmic acid for 15 min at RT. After being washed in double distilled water for 15 min the samples were dehydrated in increasing concentrations of ethanol (i.e. 70%, 96% and 100% for 15 min each), dried in a 1:1 solution of absolute ethanol and hesamethyldisilazane (HMDS) (Fluka) for 30 min and dried in pure HMDS. Samples were mounted using adhesive tape on stubs coated with a 10 nm thick layer of gold in a sputtering device (Balzers Union) and observed with a Philips XL-20 microscope at 15 keV.

3. Results

3.1. As-electrospun nanofibers

Fig. 1a shows an SEM image of gelatin nanofibers (G) electrospun from a solution of acetic acid/water. The randomly collected fibers are free of bead defects and display a relatively uniform diameter distribution. The numerous attempts to optimize cross-linking of these gelatin mats did not provide completely satisfactory results. Therefore, in order to improve the cross-linking process and thus the properties of the scaffolds we modified the composition of the electrospinning solution by adding a small amount of genipin in ethanol. The SEM image of a gelatin–genipin (GG) electrospun scaffold in Fig. 1b shows that the fibers are defect free and very regular. The fiber mean diameter is similar to that of G nanofibers, as reported in Table 2.

In order to determine gelatin structural modifications due to the electrospinning process, FTIR and XRD analyses were carried out on the electrospun scaffolds, as well as on the gelatin and gelatin–genipin films. Fig. 2 reports the FTIR spectra of gelatin films prepared from (a) aqueous solution and from (b) acetic acid/water solution, together with the spectra of G and GG electrospun scaffolds (c, d). All spectra show several absorption bands corresponding to amide A, I, II and III [28]. The spectrum of the film prepared

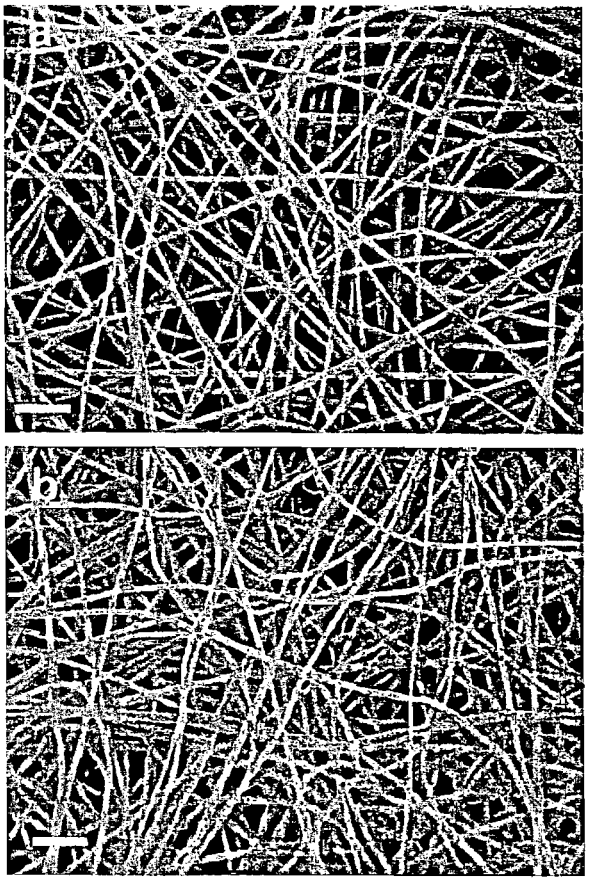

Fig. 1. SEM images of as-electrospun (a) G and (b) GG mats. Bars: 5 μm.

Table 2
Nanofiber diameters of as-electrospun and cross-linked mats (mean values ± standard deviation are reported).

Sample	Fiber diameter (nm)
G	440 ± 50
GG	460 ± 60
GG_5A	600 ± 120[a,b]
GG_7A	980 ± 180
GG_11A	940 ± 130
GG_5B	810 ± 180
G_5C7d	740 ± 120[a]
GG_5C7d	990 ± 130[c]

[a] GG_5A vs G, GG, G_5C7d vs G, GG ($P < 0.001$).
[b] GG_5A vs GG_7A, GG_11A, GG_5B ($P < 0.001$).
[c] GG_5C7d vs GG_5B, GG_5A, G_5C7d ($P < 0.001$).

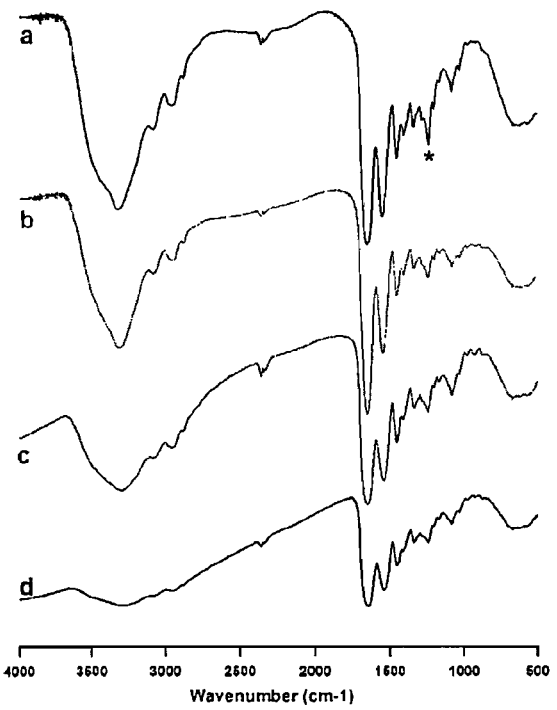

Fig. 2. FTIR absorption spectra of gelatin films prepared from (a) aqueous and (b) acetic acid/water solutions, compared with the spectra of as-electrospun (c) G and (d) GG mats. *1234 cm^{-1} band.

from gelatin–genipin in acetic acid/water is similar to that reported in Fig. 2b. With respect to the other spectra, that recorded from the film prepared from gelatin aqueous solution displays a relatively high intensity for the 1234 cm^{-1} band in the amide III region. Moreover, the spectrum of the GG scaffold, and even more that of the G scaffold, are less resolved with respect to those of the films.

Fig. 3 compares the wide angle X-ray diffraction pattern of a gelatin film prepared from (a) an aqueous solution with that of a film prepared from (b) an acetic acid/water solution, and with that recorded from (c) a GG electrospun scaffold. The pattern of the gelatin film from aqueous solution (a) shows two diffraction reflections: the first corresponds to a periodicity of about 1.1 nm and is related to the diameter of the triple helix; the second corresponds to a periodicity of about 0.45 nm and has been ascribed to the distance between adjacent polypeptide strands [29]. Patterns (b) and (c) are much less defined and show only the second broad peak.

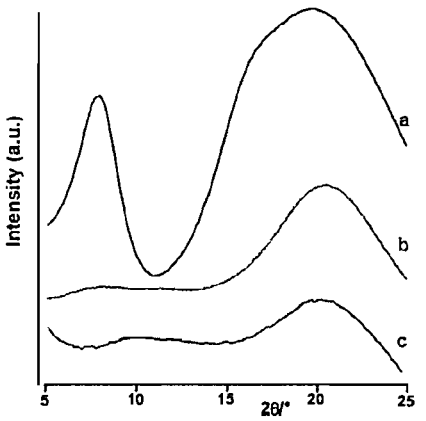

Fig. 3. XRD diffraction patterns of gelatin films prepared from (a) aqueous and (b) acetic acid/water solutions, compared with the pattern of as-electrospun (c) GG mat.

3.2. Optimization of the cross-linking conditions

The addition of genipin to the electrospinning solution did not prevent solubilization of the electrospun scaffolds when exposed to water. Therefore, the mats were submitted to further cross-linking treatments with genipin. Possible morphological modifications of the cross-linked nanofibers upon water exposure were investigated through SEM analysis of the mats air dried at 37 °C after immersion in water for 30 min.

3.2.1. Method A

Some of the GG mats were soaked in genipin solutions at different concentrations at 37 °C for 7 days. Genipin concentrations in ethanol of 5%, 7% and 11% (w/v) were tested. Fig. 4a–4c shows SEM images of the GG mats cross-linked with increasing genipin concentrations. The mean fiber diameters are significantly greater than those of the as-electrospun fibers, and increase at relatively high genipin concentration (Table 2). In the images recorded after scaffold immersion in water (Fig. 4e–4g) the fibers show a drastic morphology change with many junction zones fused together.

3.2.2. Method B

The influence of air drying temperature was tested on GG mats cross-linked with 5% genipin. In particular, the samples were dried overnight at 45 °C instead of 37 °C as in method A. The images recorded before and after water exposure (see Fig. 4d and h) show that the increase in the drying temperature does not prevent fiber fusion after water exposure.

3.2.3. Method C

Method C introduces a further step in the cross-linking procedure, rinsing the mats in 0.1 M PBS, pH 7.4, before air drying. The method was tested on mats soaked in 5% w/v genipin for two different periods of time, 3 and 7 days. The fibers in the mat GG_5C3d after rinsing in water appear fused together at most contact points (data not shown). Fig. 5 shows the morphology of the GG_5C7d fibers (a) before and (c) after exposure to water. It is evident that soaking in genipin for 7 days followed by rinsing in PBS yielded samples able to retain the morphology of the individual nanofibers after exposure to water, as enhanced in the detail shown in the inset to Fig. 5c. Fig. 5b and d reports the SEM images of G_5C7d before and after rinsing in water. Fig. 5d shows that even those fibers electrospun from gelatin solution in the absence of genipin retain their morphology after rinsing in water, although in this case parts of the junction zones appear fused together.

附件二

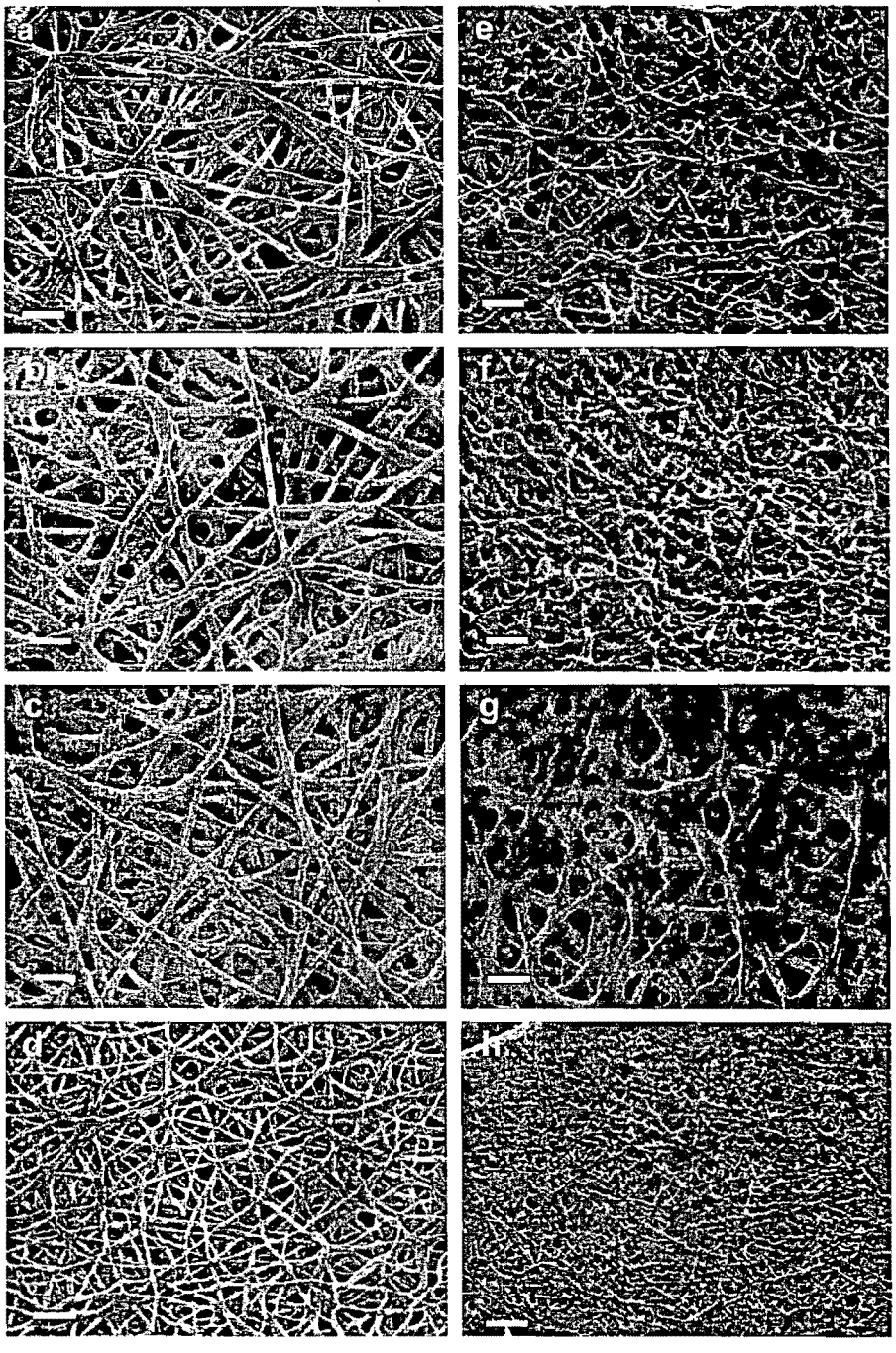

Fig. 4. SEM images of GG mats cross-linked according to method A (a)–(c) before and (e)–(g) after rinsing in water. (a, e) 5%, (b, f) 7% and (c, g) 11% genipin solution. The images of GG mats cross-linked according to method B (d) before and (h) after rinsing in water are also reported. Bars: (a)–(c), (e)–(g), 5 μm; and (d, h), 10 μm.

The morphological characterization of both the G_5 and GG_5 scaffolds indicate that the conditions utilized in the method C procedure gave the best results in terms of stabilization of the mats against water solubilization. As a consequence, this procedure was selected as the best method to cross-link electrospun gelatin scaffolds with genipin, and GG_5C7d, as well as G_5C7d as a control sample, were submitted to further characterization.

3.3. Degree of cross-linking and stability in solution

The stability of the scaffolds prepared according to method C was further tested by investigating fiber morphology modifications after immersion in cell culture medium (DMEM) for 7 days. The SEM images reported in Fig. 6a and b show no undesired alteration of the nanofibers, which exhibit only a slight reduction in their

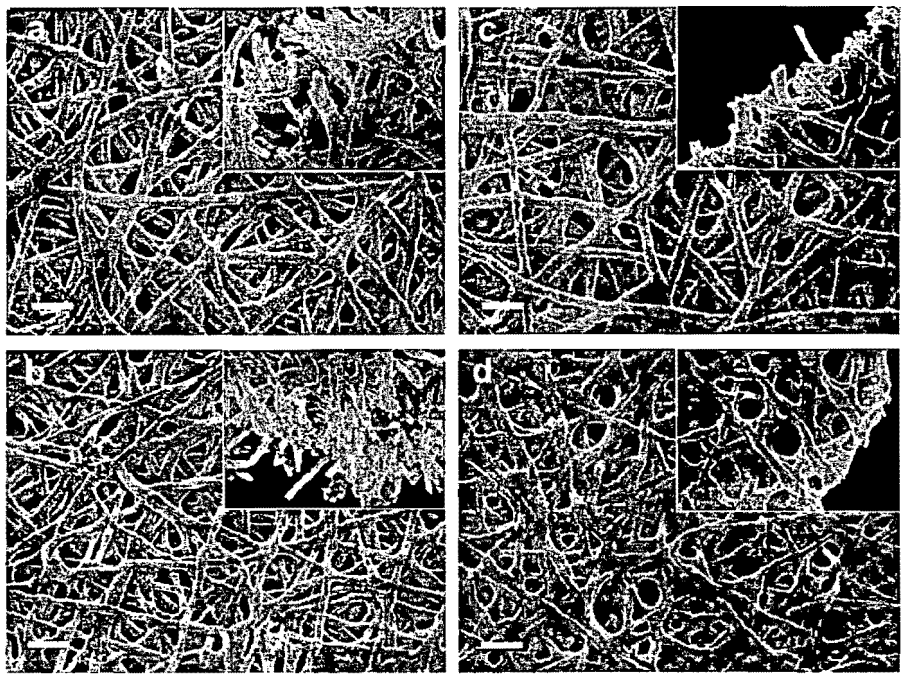

Fig. 5. SEM images of (a, c) GG and (b, d) G mats crosslinked according to method C (a, b) before and (c, d) after rinsing in water. The insets report a view of a mat edge. Bars: 5 μm.

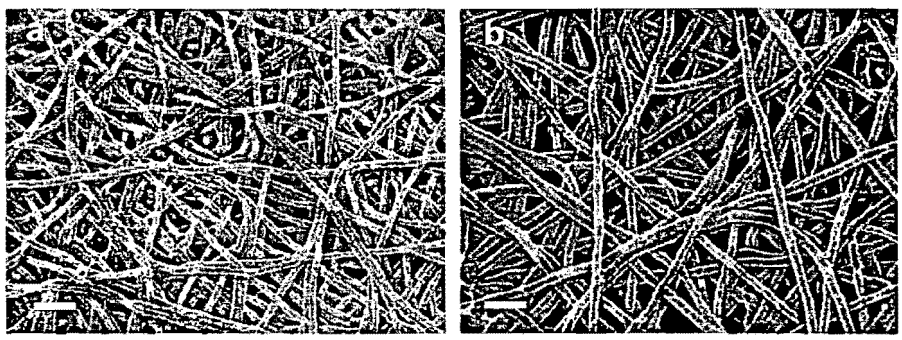

Fig. 6. SEM images of (a) G_5C7d and (b) GG_5C7d after 7 days immersion in DMEM. Bars: 5 μm.

mean diameter with respect to that measured before immersion. The mean diameters of G_5C7d and GG_5C7d after 7 days in DMEM were 720 ± 80 and 840 ± 150 nm, respectively.

The extent of cross-linking was calculated from the moles of free ε-amino groups per gram of gelatin [26]. The results indicate that GG_5C7d and G_5C7d exhibit 92 ± 5% cross-linking, whereas the value determined for the as-electrospun GG nanofibers was 15 ± 5%.

3.4. Mechanical properties

Typical tensile stress–strain curves recorded from G and GG samples before and after cross-linking are reported in Fig. 7. A dramatic modification of the mechanical behavior induced by the presence of genipin is evident in the as-electrospun mats. The stress–strain curves recorded from the different samples have been used to evaluate the Young's modulus (E), the stress at break (σ_b), and the deformation at break (ε_b) of the scaffolds. The mean values are reported in Table 3.

3.5. In vitro tests

The viability of VW-MSCs cultured on G and GG electrospun mats after 7 days culture was preliminarily assessed by SEM analysis. VW-MSCs are vital in both types of scaffolds and they retain the native mesenchymal spindle-shaped morphology, as shown in Fig. 8a and b for G_5C7d. No differences in terms of cell adhesion and morphology were observed between the two types of mats.

4. Discussion

The results of this work allowed optimization of the cross-linking conditions for electrospun gelatin nanofibers with genipin. Genipin was chosen because of its cross-linking efficiency – genipin-fixed tissues were reported to exhibit resistance to enzymatic degradation comparable with glutaraldehyde-fixed tissue [30,31] – as well as for its better biocompatibility and lower cytotoxicity compared with other cross-linking agents [32]. Previous attempts

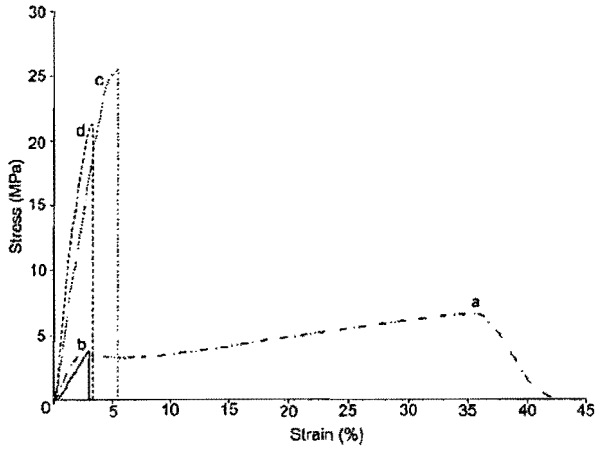

Fig. 7. Typical stress–strain curves recorded from as-electrospun (a) G and (b) GG mats and from cross-linked (c) G_5C7d and (d) GG_5C7d mats.

Table 3
Strain at break (ε_b), stress at break (σ_b), and Young's modulus (E) of as-electrospun and cross-linked mats (each value is the mean of 10 determinations reported with the standard deviation).

Sample	ε_b (%)	σ_b (MPa)	E (MPa)
G	37 ± 5[a]	6.0 ± 0.6[c]	240 ± 30[e]
GG	3.2 ± 0.5	3.8 ± 0.6	194 ± 20
G_5C7d	5.5 ± 0.3[b]	22 ± 4[d]	820 ± 100[f]
GG_5C7d	3.5 ± 0.2	20.9 ± 0.4[d]	990 ± 40[f,g]

[a] G vs GG, G_5C7d, GG_5C7d ($P < 0.001$).
[b] G_5C7d vs GG_5C7d ($P < 0.001$).
[c] G vs GG($P < 0.001$).
[d] G_5C7d vs G, GG; GG_5C7d vs G, GG ($P < 0.001$).
[e] G vs GG ($P < 0.001$).
[f] G_5C7d vs G, GG; GG_5C7d vs G, GG ($P < 0.001$).
[g] GG_5C7d vs G_5C7d ($P < 0.001$).

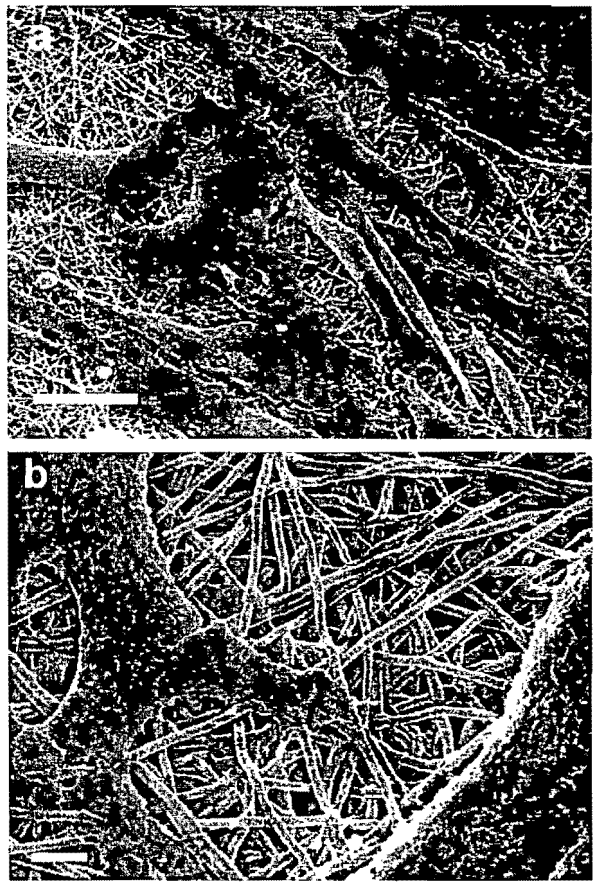

Fig. 8. SEM images of VW-MSCs grown on G_5C7d for 7 days. Bars: (a) 50 μm and (b) 5 μm.

to cross-link gelatin fibers using genipin in water/ethanol solution provoked remarkable modifications of the original fiber morphology, which was attributed to slow cross-linking kinetics compared with the rate of gelatin dissolution [19]. A novel route was recently proposed by Ko et al. [25], who incorporated genipin within gelatin nanofibers during electrospinning and demonstrated that the fibers thus obtained underwent cross-linking. However, upon water contact modification of the fiber morphology was observed.

We tested a number of different conditions in order to prevent dissolution of the mats upon water contact, but most attempts performed on electrospun gelatin scaffolds (G) were unsuccessful. Addition of a small amount of genipin to the electrospinning solution (GG) improved the results remarkably, without substantial modification of the initial fiber morphology (Fig. 1a and b). Moreover, the G and GG mats did not display significant structural differences. In fact, the FTIR spectra of the GG and G mats are quite similar and display the characteristic amide bands. The amide A band is associated with the N–H stretching mode and amide I arises from the carbonyl C=O double stretching mode, whereas amide II has been ascribed to the deformation of N–H bonds and C–H stretching and amide III corresponds to vibration in the plane of C–N and N–H groups of bound amide or vibration of CH_2 [28,33]. The reduced intensity of the absorption bands in the amide I and II regions, and even more in the amide III region, of the FTIR spectra of gelatins with respect to collagen has been associated with the loss of triple helix content during gelatin extraction [34]. The results of this paper indicate that in comparison with those of gelatin films (Fig. 2a and b) the FTIR spectra of the electrospun samples (Fig. 2c and d) display a broadening of the bands, most likely because, with respect to the smooth surface of the films, the rough and porous surface of the scaffolds affects resolution. Moreover, gelatin films prepared from aqueous solution exhibit a relative higher intensity of the absorption band at 1234 cm^{-1} in the amide III region (Fig. 2a) than the other samples, in agreement with a relatively higher content of triple helix structure. The similarity between the relative intensity of these bands in the spectra reported in Fig. 2b–d indicates that the reduction in structural order is due to the treatment with acetic acid and not to the electrospinning process. Accordingly, X-ray diffraction data indicate that the reflection at about 1.1 nm, characteristic of the triple helix structure [29], which can be appreciated in the pattern of gelatin films obtained from aqueous solution (Fig. 3a), is not appreciable in the patterns recorded from films, as well as electrospun nanofibers, prepared from acetic acid/water solutions. It must be concluded that acetic acid, as previously reported for formic acid [35], prevents the partial renaturation of gelatin that occurs during gelling from aqueous solution and implies a partial rearrangement of its structure from random coil to triple helix [36].

Genipin addition to the electrospinning solution does not prevent scaffold solubilization upon water exposure, but it improves the results of further cross-linking reaction. Treatment with genipin for 7 days at 37 °C (method A) provides much better water

resistance of GG electrospun nanofibers, even if their morphology still appears affected by water contact. Genipin cross-linking also induces a significant increase in the mean diameter of the nanofibers, in agreement with the data of Ko et al. [25]. An increase in the temperature of cross-linking (method B) was verified to induce only minor variations, whereas the results obtained on the samples cross-linked using the C method demonstrated that rinsing in PBS solution before air drying is a key factor in stabilization of the scaffolds, most probably because the ionic strength of PBS reduces gelatin swelling [37]. Cross-linked GG mats retain their morphology after water exposure, and the morphology of cross-linked G mats also appears only slightly affected by water. The nanofibers of both kinds of mats maintain a straight morphology and are not fused together after 1 week immersion in DMEM. In fact, the morphology does not appear to be altered even when VW-MSCs were cultured on the mats for 7 days. Moreover, SEM analysis of cell morphology and adhesion confirms that G and GG in the form of electrospun fiber mats are both biocompatible and able to support VW-MSCs spreading and adhesion.

Cross-linking greatly affects the mechanical properties of the scaffolds. In fact, genipin addition to the electrospinning solution induced a remarkable modification of the stress–strain curve of the resulting mat. Moreover, the strain at break of as-spun GG mats assumes a mean value significantly smaller than that measured on as-spun G mats. After cross-linking according to method C the stress at break and the Young's modulus of the G and GG mats increased remarkably, whereas the strain at break of the G scaffolds decreased significantly. Although as-spun GG mats display a degree of cross-linking of just 15 ± 5%, the significantly smaller value of ε_b and greater value of E exhibited by electrospun GG_5C7d mats with respect to G_5C7d mats indicate that genipin addition to the electrospinning solution influences the mechanical properties of the mats even after further, much more extensive, cross-linking.

5. Conclusions

The method developed in this work represents the first successful approach to prepare genipin cross-linked, bead-free electrospun gelatin nanofibers that maintain their original morphology after exposure to water. The use of genipin couples crosslinking efficiency with low toxicity, as shown by the results of preliminary in vitro tests. Moreover, the cross-linked mats display interesting and tunable mechanical properties.

Acknowledgements

This research was carried out with the financial support of MIUR and of Regione Emilia Romagna (Programma di Ricerca Regione Università 2007–2009, Area 1b "Medicina rigenerativa").

Appendix A. Figures with essential colour discrimination

Certain figures in this article, particularly Figures 2, 3 and 7, are difficult to interpret in black and white. The full colour images can be found in the on-line version, at doi:10.1016/j.actbio.2010.11.021.

References

[1] Place ES, Evans ND, Stevens MM. Complexity in biomaterials for tissue engineering. Nat Mater 2009;8:457–70.
[2] Stevens MM, George JH. Exploring and engineering the cell surface interface. Science 2005;310:1135–8.
[3] Ma PX. Biomimetic materials for tissue engineering. Adv Drug Delivery Rev 2008;60:184–98.
[4] Agarwal S, Wendorff JH, Greiner A. Use of electrospinning technique for biomedical applications. Polymer 2008;49:5603–21.
[5] Casper CL, Yang W, Farach-Carson MC, Rabolt JF. Coating electrospun collagen and gelatin fibers with perlecan domain I for increased growth factor binding. Biomacromolecules 2007;8:1116–23.
[6] Matthews JA, Wnek GE, Simpson DG, Bowlin GL. Electrospinning of collagen nanofibers. Biomacromolecules 2002;3:232–8.
[7] Rho KS et al. Electrospinning of collagen nanofibers: effects on the behavior of normal human keratinocytes and early-stage wound healing. Biomaterials 2006;27:1452–61.
[8] Torres-Giner S, Gimeno-Alcañiz JV, Ocio MJ, Lagaron JM. Comparative performance of electrospun collagen nanofibers cross-linked by means of different methods. ACS Appl Mater Interfaces 2009;1:218–23.
[9] Zhang YZ, Venugopal J, Huang ZM, Lim CT, Ramakrishna S. Crosslinking of the electrospun gelatin nanofibers. Polymer 2006;47:2911–7.
[10] Bigi A, Cojazzi G, Panzavolta S, Roveri N, Rubini K. Stabilization of gelatin films by crosslinking with genipin. Biomaterials 2002;23:4827–32.
[11] Mano JF et al. Natural origin biodegradable systems in tissue engineering and regenerative medicine: present status and some moving trends. J R Soc Interface 2007;4:999–1030.
[12] Li M, Mondrinos MJ, Gandhi MR, Ko FK, Weiss AS, Lelkes PI. Electrospun protein fibers as matrices for tissue engineering. Biomaterials 2005;26:5999–6008.
[13] Huang ZM, Zhang YZ, Ramakrishna S, Lim CT. Electrospinning and mechanical characterization of gelatin nanofibers. Polymer 2004;45:5361–8.
[14] Gu SY, Wang ZM, Ren J, Zhang CY. Electrospinning of gelatin and gelatin/poly(L-lactide) blend and its characteristics for wound dressing. Mater Sci Eng C 2009;29:1822–8.
[15] Song JH, Kim HE, Kim HW. Production of electrospun gelatin nanofiber by water-based co-solvent approach. J Mater Sci Mater Med 2008;19:95–102.
[16] Bigi A, Bracci B, Cojazzi G, Panzavolta S, Roveri N. Drawn gelatin films with improved mechanical properties. Biomaterials 1998;19:2335–40.
[17] Rault I, Frei V, Herbage D, Abdul-Malak N, Huc A. Evaluation of different chemical methods for cross-linking collagen gel, films and sponges. J Mater Sci Mater Med 1996;7:215–21.
[18] Khor E. Methods for the treatment of collagenous tissues for bioprostheses. Biomaterials 1997;18:95–103.
[19] Sisson K, Zhang C, Farach-Carson MC, Chase DB, Rabolt JF. Evaluation of cross-linking methods for electrospun gelatin on cell growth and viability. Biomacromolecules 2009;10:1675–80.
[20] Olde Damink LHH, Dijkstra PJ, Van Luyn MJA, Van Wachem PB, Nieuwenhuis P, Feijen J. Glutaraldehyde as a crosslinking agent for collagen-based biomaterials. J Mater Sci Mater Med 1995;6:460–72.
[21] Sung HW, Huang DM, Chang WH, Huang LL, Tsai CC, Liang IL. Gelatin-derived bioadhesives for closing skin wounds: an in vivo study. J Biomater Sci Polym Ed 1999;10:751–71.
[22] Sung HW, Huang DM, Chang WH, Huang RN, Hsu JC. Evaluation of gelatin hydrogel crosslinked with various crosslinking agents as bioadhesives: in vitro study. J Biomed Mater Res 1999;46:520–30.
[23] Sung HW, Liang IL, Chen CN, Huang RN, Liang HF. Stability of a biological tissue fixed with a naturally occurring crosslinking agent (genipin). J Biomed Mater Res 2001;55:538–46.
[24] Kim MS, Jun I, Shin YM, Jang W, Shin H. The development of genipin-crosslinked poly(caprolactone) (PCL)/gelatin nanofibers for tissue engineering applications. Macromol Biosci 2010;10:91–100.
[25] Ko J, Yin HY, An J, Chung D, Kim JH, Lee S, et al. Characterization of cross-linked gelatin nanofibers through electrospinning. Macromol Res 2010;18:137–43.
[26] Ofner III CM, Bubnis WA. Chemical and swelling evaluations of amino group crosslinking in gelatin and modified gelatin matrices. Pharm Res 1996;13:1821–7.
[27] Pasquinelli G et al. Multidistrict human mesenchymal vascular cells: pluripotency and stemness characteristics. Cytotherapy 2010;12:275–87.
[28] Hashim DM, Che Man YB, Norakasha R, Shuhaimi M, Salmah Y, Syahariza ZA. Potential use of Fourier transform infrared spectroscopy for differentiation of bovine and porcine gelatins. Food Chem 2010;118:856–60.
[29] Okuyama K. Revisiting the molecular structure of collagen connective tissue. Tissue Res 2008;49:299–310.
[30] Sung HW, Huang RN, Huang LLH, Tsai CC, Chiu CT. Feasibility study of a natural crosslinking reagent for biological tissue fixation. J Biomed Mater Res 1998;42:560–7.
[31] Huang LL, Sung HW, Tsai CC, Huang DM. Biocompatibility study of a biological tissue fixed with a naturally occurring crosslinking reagent. J Biomed Mater Res 1998;42:568–76.
[32] Tsai CC, Huang RN, Sung HW, Liang HC. In vitro evaluation of the genotoxicity of a naturally occurring crosslinking agent (genipin) for biologic tissue fixation. J Biomed Mater Res 2000;52:58–65.
[33] Bergo P, Sobral PJA. Effects of plasticizer on physical properties of pigskin gelatin films. Food Hydrocolloids 2007;21:1285–9.
[34] Muyonga JH, Cole CGB, Duodu KG. Extraction and physico-chemical characterisation of Nile perch (*Lates niloticus*) skin and bone gelatin. Food Hydrocolloids 2004;18:581–92.
[35] Ki CS, Baek DH, Gang KD, Lee KH, Um IC, Park YH. Characterization of gelatin nanofiber prepared from gelatin–formic acid solution. Polymer 2005;46:5094–102.
[36] Ross-Murphy SB. Structure and rheology of gelatin gels: recent progress. Polymer 1992;33:2622–7.
[37] Veis A. The macromolecular chemistry of gelatin. New York: Academic Press; 1964.